Journal of Materials Chemistry A

Accepted Manuscript

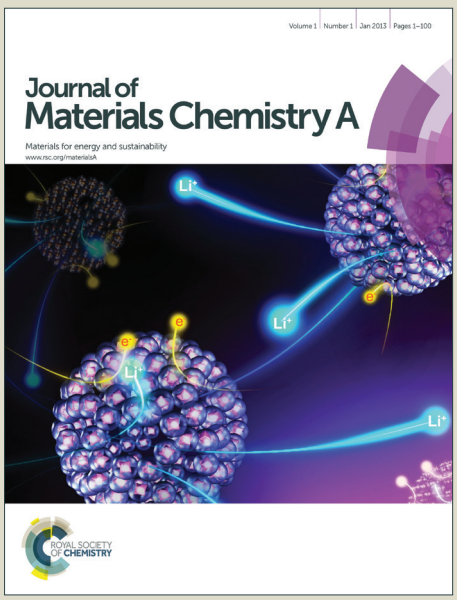

ROYAL SOCIETY OF CHEMISTRY

www.rsc.org/materialsA

Journal Name

RSCPublishing

ARTICLE

Implications of TiO_2 Surface Functionalization on Polycrystalline Mixed Halide Perovskite Film and Photovoltaic Devices

Cite this: DOI: 10.1039/x0xx00000x

Received 00th January 2012,
Accepted 00th January 2012

DOI: 10.1039/x0xx00000x

www.rsc.org/

Valentino L. P. Guerra,[a] Davide Altamura,[b] Vanira Trifiletti,[a,c] Silvia Colella,[a] Andrea Listorti,[c] Roberto Giannuzzi,[c] Giovanna Pellegrino,[d] Guglielmo Guido Condorelli,[e] Cinzia Giannini,[b] Giuseppe Gigli[a,f] and Aurora Rizzo[f]*

We exploit TiO_2 surface functionalization as a tool to act on the crystallization process of $CH_3NH_3PbI_{3-x}Cl_x$ perovskite thin films resulting in a reduction of the degree of orientation along the (110) crystallographic planes. Notably, the variation of the film crystalline orientational order does not affect the photovoltaic performances of the perovskite-based devices, whose efficiency remains mostly unchanged. Our findings suggest that other factors are more significant in determining the device efficiency, such as the non-homogenous coverage of the TiO_2 surface causing charge recombination at the organic/TiO_2 interface, defect distribution on the perovskite bulk and at the interfaces, and transport in the organic or TiO_2 layer. This observation represents a step towards the comprehension of the perovskite film peculiarities influencing the photovoltaic efficiency, for high performing devices.

Introduction

Organic-inorganic hybrid perovskites are among the most exciting and successful light-harvesting materials for photovoltaic applications.[1,2] Hybrid 3D perovskite structure consists of an inorganic framework of corner sharing octahedra and organic cations filling the 12-fold coordinated voids.[3] The formation of hybrid perovskites occurs spontaneously upon the mixing of two precursors, lead halide and methylammonium (MA) halide salts, onto the substrate. As generally occurs in self-assembly processes, the environment conditions and substrate are of paramount importance to control perovskite formation and, consequently, final device performance.[4-9]
Unlike other composite materials where inorganic and organic components are often either randomly arranged or show a short-range order, hybrid perovskites can potentially organize in a long-range ordered crystal structure.[10,11] Namely, it has been recently demonstrated that (110) planes of MA lead halide perovskite can be highly oriented parallel to the substrate surface.[6,7,12,13] Considering this peculiar property, controlling the crystallization process of perovskite materials is regarded as a crucial step toward high performing devices and a fine tuning of the crystalline order in perovskite film is deemed necessary to correlate the material structure and the charge photo-generation.[12] However, the effective impact of the perovskite crystal orientation and structure on the photovoltaic performance are still under debate and not fully understood.[6,7,13,14] What appears to be clear in the current scenario is the active role of the substrate in inducing certain properties to the perovskite layer by directly influencing the nucleation process through specific interactions. This is true especially in the case of mixed halide perovskite, where the formation of the final material occurs over a relatively long time due to a non-stoichiometric ratio of the precursors. In this frame, Kirmayer et al. have demonstrated the presence of $PbCl_2$ nanocrystals during the $MAPbI_{3-x}Cl_x$ formation process, acting as heterogeneous nucleation sites for the growth of perovskite crystals.[15] In addition, we have recently proven that the chloride anion in $MAPbI_{3-x}Cl_x$ perovskites preferentially locates in close proximity of the interface with TiO_2 compact layer, due to an increased chloride-TiO_2 affinity.[16,17] Starting from these observations, we envisage the possibility to interfere with the perovskite polycrystal nucleation, which should occur at the TiO_2 surface, by a facile TiO_2 functionalization. While Eperon et al. have shown that the interaction of $MAPbI_{3-x}Cl_x$ with the TiO_2 layer dictates the film morphological properties,[18] and while widely employed for improving the power conversion efficiency (PCE) of thin film solar cells, interfacial engineering between electrodes and perovskite has only peripherally been explored.[19] Surface functionalization with some aminoacids has been deployed onto mesoporous TiO_2 substrate for $CH_3NH_3PbI_3$ perovskite,[20] with the aim of passivating surface traps on titania and promoting electron injection. The anchoring groups also determined a better growth of perovskite networks and uniform crystalline plain. Here, we report on the TiO_2 surface functionalization with either n-dimethyloxamic acid (DMOA) or sodium phosphonoformate tribasic hexahydrate (NaPTH) to reduce the orientation of the (110) perovskite lattice planes. We found that $MAPbI_{3-x}Cl_x$ perovskite on bare

TiO_2 shows a high degree of 110 orientation, whereas $MAPbI_3$ presents randomly oriented polycrystals. The functionalization with DMOA or NaPTH results in a partial or complete disruption of the $MAPbI_{3-x}Cl_x$ preferred orientation. By surface analysis, we found that NaPTH covers the surface of TiO_2, while the DMOA passivation is poor and consequently less effective in screening the perovskite precursors/TiO_2 interaction. Comparing the device performances of the three $MAPbI_{3-x}Cl_x$ based devices under study, along with the $MAPbI_3$ reference, we found that the PCE is not affected by the TiO_2 surface functionalization, suggesting that the orientation of the (110) planes may not be the determining factor to improve photovoltaic performance.

Experimental Section

TiO_2 compact layer deposition and functionalization. Fluorine-doped tin oxide FTO glass substrates (Pilkington, TEC15, 15 Ohm/sq) were partially etched with metallic Zn and HCl 2M. They were washed with water and cleaned in an ultrasonic bath in acetone and isopropanol for 10 min each. Then they were immersed into a TL1 washing solution ($H_2O/NH_3/H_2O_2$ 5:1:1, v/v) and heated to 80 °C for 15 min to remove organic contamination. To make a compact TiO_2 blocking layer of ~80 nm, the cleaned FTO glasses were coated with 0.15 M titanium diisopropoxidebis(acetylacetonate) (75% Aldrich) in 1-butanol (Aldrich) solution by the spin-coating (3000 rpm), then heated at 125 °C for 5 min. After the coated film was cooled down to the room temperature, the same process was repeated again in the same way. After the last cooling to room temperature the process was repeated with 0.3 M titanium diisopropoxidebis(acetylacetonate) solution in 1-butanol at 3000 rpm. The as coated FTO substrates with TiO_2 precursor solutions finally underwent a sintering process at 520 °C for 2 hours. N-dimethyloxamic acid (DMOA) and sodium phosphonoformate tribasic hexahydrate (NaPTH) were purchased from Aldrich. For functionalization, the as prepared TiO_2 substrates were immersed in 0.5 mM ethanol solution of either the carboxylic or phosphonic acid for 18 h. The modified TiO_2 substrates were then rinsed by ethanol, blow-dried with nitrogen gas.

Methyl ammonium lead iodide chloride perovskite preparation. Mixed halide hybrid perovskite are prepared by self-organization processes using $PbCl_2$ (Aldrich) and methylammonium iodide MAI precursor solutions (20 wt%) obtained by dissolving MAI and $PbCl_2$ (3:1 molar ratio) in anhydrous N,N-Dimethylformamide (DMF) at room temperature. The intermediate MAI compound was prepared by reactions of the amine, CH_3NH_2 (41%) (Fluka), aqueous solutions with HI (57%, Aldrich), as previously reported. All the reagents were used as purchased without further purification.[21]

X-ray Photo-electron spectroscopy (XPS). XPS analyses have been performed by using a PHI ESCA/SAM 5600 Multy technique spectrometer equipped with a Mg Kα X-ray source at a pressure of 5x10-9 Torr. Measurements have been performed at take off angle (angle between the surface of the sample and the detector) of 45° with an angular acceptance of ±5°. The binding energy (BE) scale was calibrated by centring the C 1s signal due to the adventitious/ hydrocarbon carbon at 285.0 eV.

Grazing Incidence wide angle X-ray scattering (GIWAXS) and X-ray Diffraction (XRD). GIWAXS measurements were performed at the XMI-L@b with a Rigaku (GI)SAXS/(GI)WAXS laboratory set-up,[22] equipped with a FR-E+ microsource and a SMAX3000 3-pinholes camera. The experimental settings were: 1° incidence angle and 0.154 nm radiation wavelength. The patterns were calibrated by using a standard Silver Behenate powder sample. Data were collected on an image plate (IP) detector with 100 μm pixel size at 87 mm sample-to-detector distance. XRD data were collected in coupled sample-detector scan mode (θ/2θ) on a D8 Discover (Bruker) equipped with a Göbel mirror for Cu-Kα radiation and a scintillator detector.

UV-Vis absorption and morphological characterization. Film absorbance spectra were measured by a Varian Cary 5000 spectrophotometer in reflectance mode. The scanning electron microscopy (SEM) imaging was performed by the MERLIN Zeiss SEM FEG instrument at an accelerating voltage of 5 kV using an In-lens detector.

Device fabrication and testing. In order to get an extremely ordered polycrystalline film, a warm (60°C) precursor solution 20 wt% $MAPbI_{3-x}Cl_x$ was deposited by spin-coating on pre-heated (120°C) TiO_2 compact layer at 1000 rpm for 45 seconds, followed by annealing at 100°C for 1 h. The same procedure has been followed also for the substrates functionalized by DMOA or NaPTH functionalized TiO_2. A chlorobenzene solution containing 131 mM Spiro-OMeTAD, 216 mM tert-butylpyridine and 58 mM lithium bis(trifluoromethylsyfonyl)imide salt was spin-coated onto the perovskite. Solar cell devices were completed by thermal evaporation of 200 nm Ag electrodes and left 3 hours in ambient air. The step voltage was fixed at 10 mV and the delay time, which is a set delay at each voltage step before measuring each current, was 500 ms. I-V curves for all devices were measured by masking the active area with a black mask of 0.09 cm^2 in ambient air.

Electrochemical Measurements. Electrochemical experiments were carried out with an Autolab Potentiostat PGSTAT 302N interfaced with a personal computer. A standard three electrode electrochemical cell with a Pt gauze counter electrode and a silver wire as quasi-reference electrode. The TiO_2 modified electrode with a geometric area of 1 cm^2 served as working electrode. Acetonitrile solutions with 0.1 M $LiClO_4$ as supporting electrolyte were used and the cyclic voltammograms were obtained at 20 mVs^{-1}. It was bubbled with Ar at least for 20 min and Ar was blown over the electrolyte during the measurement.

Time correlated single photon counting. Time resolved photoluminescence measurements were performed using time-correlated single-photon counting (TCSPC) apparatus of Hamamatsu FL980, 100 ps time resolution with deconvolution analysis.

Results and discussion

The deposition process of the perovskite layer, involving crystallization by self-assembly of the components during the drying phase of the film, occurs in a two-step process: a slow nucleation and a faster growth. It is well established in literature that in the so-called mixed halide perovskite ($MAPbI_{3-x}Cl_x$) the amount of chloride in the final material is very small (surely below 4%) so that it could be considered a doping agent. It has been hypothesized that, albeit in such a small quantity, the Cl influences the electrical properties of the material, but its presence in the crystalline structure is not clear yet.[5,12,13,15-17] Nevertheless, it has also clearly been evidenced its crucial role in affecting the growth on the polycrystalline film.[23] In particular, the halide composition is regarded as the key factor in determining the nature of the nucleation event, via specifically modifying the interaction with the substrate and via slowing down the perovskite crystal formation (for a gradient in chloride concentration through the precursor solution).[16, 17, 24-26] Aiming at better clarifying this picture, here we intentionally discontinued the direct contact between substrate surface and mixed perovskite precursor solution, by modifying the TiO_2 surface with either DMOA or NaPTH molecules. Molecular modification by

phosphonic acids self-assembled onto TiO_2 has been widely reported for dye-sensitized solar cells.[27,28] Most of the molecules commonly employed, however, affect the polarity of the functionalized substrate, whereas the NaPTH molecule, because of its chemical nature, retains the TiO_2 hydrophilicity and therefore good wettability by DMF solvent. Contrarily, the DMOA dramatically improves the wettability of TiO_2. We verify the anchoring of the molecules on the TiO_2 films by observing the variation in the measured contact angle, that is smaller with respect to the naked TiO_2[29] (Figure S1 in Supporting Information). The molecules anchored on the substrate likely redistribute the chloride concentration in the precursor drop during the solution dewetting and perovskite self-assembly processes. A simplified sketch to schematize the proposed mechanism is reported in Figure 1.

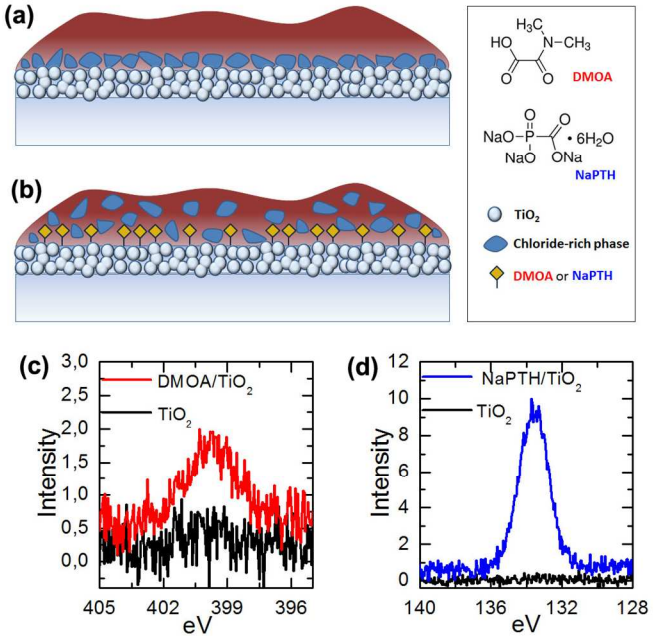

Fig. 1 Simplified sketch of the state of the perovskite precursor solution as cast onto TiO_2 in (a) absence and (b) presence of functionalizing molecules. (a) As soon as the precursor are deposited on the substrate, the specific Cl-oxide interaction could leads to the positioning of the chloride rich-phase onto TiO_2 proximity. (b) In presence of functionalizing molecules the chloride-rich phase could be redistributed in the precursor drop. Inset: molecular structure of the DMOA and NaPTH molecules together with a legend of the drawn. (c) XPS N1s region as appears in the spectra of the bare TiO_2 substrate (black line) and of the DMOA functionalized TiO_2 surface (red line). (d) XPS P2p region observed in the spectra of (black line) the bare TiO_2 and in that of (blue line) the NaPTH functionalized TiO_2.

The TiO_2 surface modification has been monitored by XPS measurements. In Fig. 1c-1d the diagnostic regions of nitrogen and phosphorous are presented and compared with those of the naked TiO_2 substrate. The nitrogen region in the spectrum of the DMOA/TiO_2 sample shows a peak centred at 399.6 eV, compatible with the presence of the amide group.[30] The spectrum of the NaPTH/TiO_2 samples shows a signal centred at 133.5eV attributed to phosphonate species.[31] In the spectra of the DMOA/TiO_2 and NaPTH/TiO_2, N/Ti x 100 and P/Ti x 100 atomic ratios are ~2 and ~9 respectively, thus indicating that the surface amount of NaPTH is notably higher than that of DMOA. As support of this, negligible differences emerge in the O1s region between the spectra of the bare substrate and the DMOA functionalized substrate showing a main signal at 530.3 eV (TiO_2) and a band at 532.1 eV (Ti–OH).[32] The presence of phosphonate on the NaPTH/TiO_2 surface is also supported by the component at 531.5 eV[31] in the O1s region (Fig. S2). The C1s region shows the reduction of the carbonates on the TiO_2 surface after the process of functionalization (Fig. S2).

The differently functionalized samples were analysed by means of grazing incidence wide angle scattering (GIWAXS) for the investigation of the crystallinity and texture of the thin films.

The recorded GIWAXS patterns for the perovskite films prepared on bare TiO_2 and either DMOA or NaPTH-functionalized TiO_2 are presented in Figure 2 a-c, respectively. The most intense diffraction peak of the mixed perovskite material is readily recognized as the inner ring (110), at approximately 1 $Å^{-1}$ (corresponding to $2\theta = 14°$). The pattern of the perovskite on bare TiO_2 (Fig. 2a) features a modulation of the scattering intensity along the rings, in particular the (110) and (220) ones, as well as on the other rings, being the maximum intensity of the (110) peak located around the direction perpendicular to the sample plane (q_z axis). As a consequence, the (110) crystallographic planes, and hence the long axis of the tetragonal perovskite crystallites, are preferentially oriented parallel to the substrate. On the other hand the in-plane orientation of the crystallites is still basically random. With the aim of disrupting the existing order, $MAPbI_{3-x}Cl_x$ was deposited on either DMOA or NaPTH-functionalized substrates. The DMOA-TiO_2 sample (Fig. 2b) also shows a certain modulation of the scattering intensity along the rings, albeit less intense. NaPTH-TiO_2 sample (Fig. 2c) shows absence of order; the two intense lobes are due to scattering from the substrate (the GIWAXS pattern of the bare substrate is reported in the Supporting material as a reference, Fig. S3). A quantitative comparison of the degree of (110) orientation of the samples is represented in Fig. 2d, where the intensity distribution along the azimuthal angle (i.e. along a ring with radius equal to a given q-value) is reported for the 110 ring of the GIWAXS maps. It is readily recognized that the 110 intensity distribution is very narrow for the bare TiO_2, whereas it is basically flat (i.e. no preferred orientation) for the NaPTH-TiO_2 sample. The degree of orientation of the DMOA-TiO_2 sample is intermediate between the other two samples.

As a comparison, we report the 2D GIWAXS map of full iodide perovskite $MAPbI_3$ film onto naked TiO_2 (Figure S4). The $MAPbI_3$ features a uniform distribution along the rings and a flat intensity distribution along the azimuthal angle, which means no preferred orientation.

In Fig. 2e, the $\theta/2\theta$ scan on the 110 diffraction peak is reported for the three samples. Due to the significant difference in the diffracted intensity, the square root of the intensity has been plotted to allow a better visibility. From the integral breath β (peak area divided by the peak maximum) of the peaks, the average grain size was derived along the [110] direction as $1/\beta$.33 The crystallite size was found to follow the same trend as the orientation degree, i.e. to decrease from the bare TiO_2 (48 nm) to the DMOA-TiO_2 (38 nm), down the NaPTH-TiO_2 sample (29 nm). It is worth to note that the derived size values represent a lower limit for the actual crystallite size, as the instrumental and strain contributions to peak broadening were neglected, so that the observed trend is meaningful rather than the absolute size values.

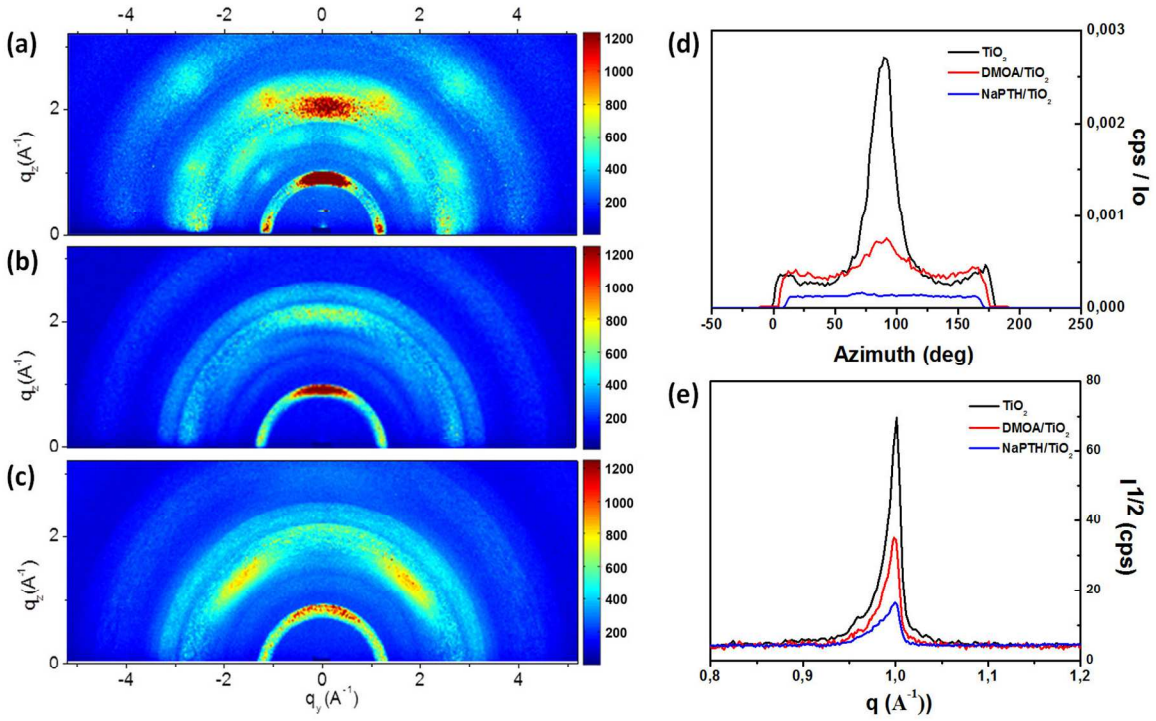

Fig. 2 GIWAXS 2D maps for the perovskite films prepared on naked TiO_2 (a) DMOA-TiO_2 (b) and NaPTH-TiO_2 (c), and relevant intensity distributions along the (110) rings (d); (110) diffraction peak is collected in 2θ/θ scan mode for both samples (e).

According to Jen et al.,[24] for the mixed halide $CH_3NH_3PbI_{3-x}Cl_x$ perovskite the self-assembly process is guided by the formation of a chloride rich intermediate phase, which drives the nucleation and growth in chloride perovskite. They propose that such an intermediate chloride rich phase locates in close proximity of the substrate, coherently with our previous report.[16] In this hypothesis, MA^+ and I^- ions in the droplet diffuse into these structural templates and, following a partial volatilization of chloride, lead to the formation of an iodide rich phase and growth of perovskite polycrystalline film. They suggest that the templating function of $MAPbCl_3$ has a paramount importance in the formation of a long-range ordered mixed halide chloride based perovskite. In addition, Kirmayer et al.[15] demonstrated that, due to the low solubility,[12] $PbCl_2$ nanocrystals are present during the fabrication process, acting as heterogeneous nucleation sites for the formation of perovskite crystals, further confirming the important role of chloride in the course of crystallization. In our system, when the TiO_2 is not functionalized, the specific Cl/TiO_2 interaction likely leads to the migration of $PbCl_2$ seeds to the substrate surface,[15,16] where the formation of the intermediate phase occurs and the oriented crystallization propagates onwards. This is as well in agreement with a recent report, in which the oriented growth of perovskite has been proposed to occur through the attachment of nuclei along a preferred crystallographic direction in an oriented attachment fashion,[12] which is well established in all-inorganic nanostructures grown from solutions.[34] As soon as the TiO_2 is functionalized with either DMOA or NaPTH molecule, the specific interaction could be screened and the templated self-assembly process starting from the TiO_2 surface is likely to be less effective.

Fig. 3 shows the impact of surface functionalization on morphological properties of the final perovskite films. From SEM inspection the morphologies of the perovskite onto naked and either DMOA or NaPTH functionalized TiO_2 are similar.

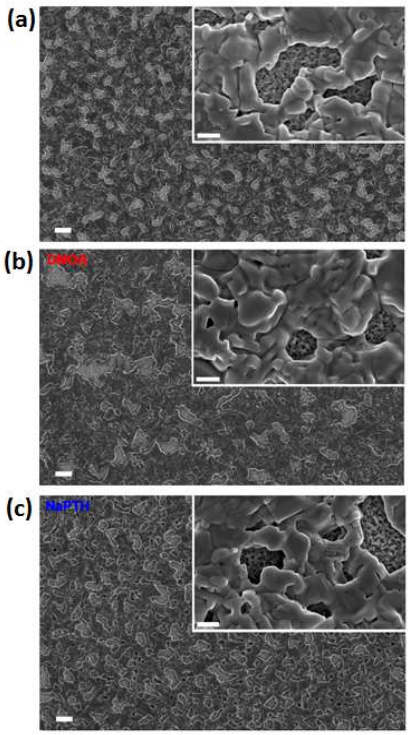

Fig. 3 Scanning electron microscopy top view images of the perovskite deposited onto (a) naked TiO2, and either (c) DMOA or (b) NaPTH functionalized TiO2 (scale bar 2 µm). The inset in the top right corner provides a magnified view of the perovskite films (scale bar 500 nm).

Overall, the DMOA-TiO_2 sample shows larger perovskite domains, possibly due to the improved wettability (see contact angle measurements in Fig. S1 of the Supporting Information). However, SEM imaging can hardly give information on the polycrystal orientation, if polycrystalline domains are smaller than a few microns. Moreover, we observe that only a minimal difference in the absorption profile and intensity can be gathered for the perovskite deposited onto either DMOA or NaPTH functionalized TiO_2 (Fig. S4 of the Supporting Information).

The perovskite films onto bare TiO_2 and functionalized with either DMOA or NaPTH are tested in conventional flat solar cell architecture: glass/FTO/TiO_2/$CH_3NH_3PbI_{3-x}Cl_x$/Spiro-OMeTAD /Ag. Figure 4 compares the representative J-V curves of functionalized and bare TiO_2 based devices, measured with a 500 ms scanning delay in reverse mode under standard air-mass 1.5 global (AM 1.5G) illumination.

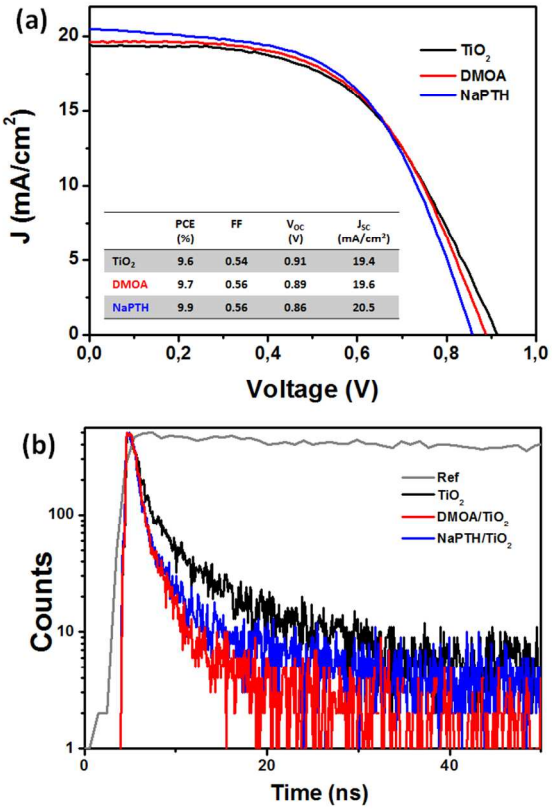

Fig. 4 (a) Current density under illumination for devices made with $CH_3NH_3PbI_{3-x}Cl_x$ onto bare TiO_2 and either DMOA or NaPTH functionalized TiO_2. (b) Radiative decays of $CH_3NH_3PbI_{3-x}Cl_x$ on bare TiO_2 or either DMOA or NaPTH functionalized TiO_2 collected at 770 nm while exciting at 645 nm. Exponential decays have been fitted with a stretched exponential function giving the following lifetimes: 600 ns for Glass/perovskite/PMMA sample, 8 ns for perovskite on bare TiO_2, 6 ns for perovskite on DMOA and NaPTH functionalized TiO_2.

The complete data report for all of the device tested, along with FF, V_{OC}, J_{SC}, PCE mean values and standard deviations are reported in Figure S6 and S7. It can be readily noted that differences in the device performances between naked TiO_2 and NaPTH/DMOA functionalized TiO_2 falls into the experimental error. The large statistical distribution of our devices can be ascribed either to the poor coverage of the TiO_2 (see SEM imaging in Figure 3) as well as to the intrinsic poor reproducibility of the perovskite thin film processed from solution. The poor coverage can indeed cause losses in the FF and J_{SC} due to recombination at the TiO_2/ spiro-OMeTAD interface and the moisture sensitivity of perovskite or uncontrollable variation in doping/oxygenation procedure can lead to a huge fluctuation of device performance.[6, 35-38] Nevertheless, the large number of fabricated devices as well as the statistical distribution of the device performances confidently allow to exclude a significant difference in the photovoltaic parameters due to the TiO_2 functionalization.

In order to address this peculiar behaviour we investigate the effect of surface functionalization on the electrochemical characteristics of the bare TiO_2 and of the either DMOA or NaPTH functionalized TiO_2. Figure S8 shows the current response of ferrocene $Fe(C_5H_5)_2$ in solution onto bare and modified TiO_2 surfaces. The redox potential is observed in a range in which the TiO_2 electrode behaves as an insulator rather than as a metal.[39] The peak potentials of NaPTH and DMOA modified films are not shifted compared to the unmodified electrode. The peak current are ~137 μAcm^{-2} for the unmodified TiO_2 electrode, ~111 μAcm^{-2} for NaPTH modified film and ~92 μAcm^{-2} for DMOA modified film. The change in anodic current between modified and unmodified film is too low to conclude that the TiO_2 surface modification slows down the charge-transfer kinetics.[40]

A further insight into the effect of the surface functionalization on the perovskite film properties is given by time resolved photoluminescence (PL) spectroscopy.[41] In Figure 4b the radiative decays recorded for the three working devices are reported, after exciting and collecting light from the substrate side of the sample. The decays are compared to a reference signal obtained by sandwiching the mixed halide perovskite between non-extracting materials such as glass and Poly(methyl methacrylate) (PMMA). For all devices a very efficient PL quenching, above 98%, is observed and only a very a small difference can be observed between them (PL lifetimes: ref ≈ 600 ns, TiO_2-untreated ≈ 8 ns, TiO_2-NaPHT or DMOA treated ≈ 6 ns), coherently with the similar device performances. A slight shortening of the PL decay is observed when DMOA or NaPTH are present on the TiO_2 surface. The difference could in part account for improved charge extraction from perovskite film in presence of functionalizing molecules leading to slightly higher photocurrent. However, the differences are very little to strongly support the point and to allow further speculations. The electrochemical and PL quenching analysis are in line with the device performance.

We can conclude that other factors are determinant in limiting and influencing the device efficiency rather than the crystalline orientation with respect to the substrate in the system, such as the poor transport in the organic layer (Spiro-OMeTAD) or TiO_2 and photo-generated charge recombination at the organic/TiO_2 interface due to poor perovskite substrate coverage or defect distribution on the perovskite bulk and at the interfaces. We suggest that improving the device configuration, by means of novel and highly conductive hole and electron transport layers or by improving perovskite surface coverage and increase its crystallite dimension could allow discriminating and exploiting the effect of polycrystal orientation on device performances.

For the sake of comparison, we also fabricated a planar device with randomly oriented and high coverage $MAPbI_3$, which represent our standard of efficiency (~15%) Figure 5. Random orientation of $MAPbI_3$ is in accordance with other studies for double step[42] and single step[43] deposited full iodide perovskite. The obtainment of a significantly high efficiency for $MAPbI_3$,

showing a completely random orientation (see Fig. S4), further evidences that high orientation may be not fundamental for photovoltaic applications.

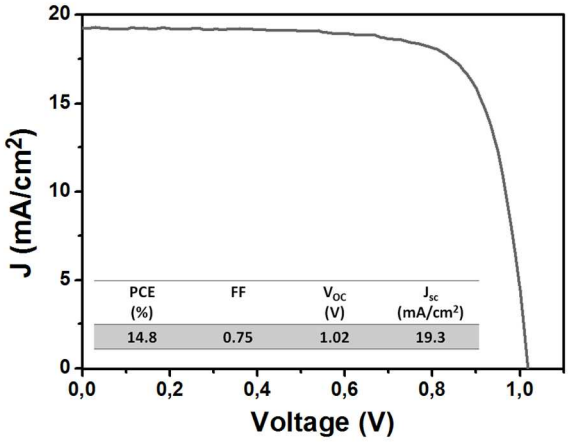

Fig. 5 (a) Current density under illumination for high efficiency device made with $CH_3NH_3PbI_3$ as active layer onto flat bareTiO_2.

Conclusions

In conclusion, we explored the TiO_2 surface functionalization as a specific way to act on the $CH_3NH_3PbI_{3-x}Cl_x$ perovskite growth and to modify polycrystalline order of the deposited film, from highly to randomly oriented crystals. We found a strict relationship between the TiO_2 coverage of the functionalizing molecules and the crystalline orientation of the perovskite film. We propose two possible factors influencing the kinetics of the perovskite growth onto the functionalized substrate, and therefore its crystalline order: a) the modification of the surface properties that affects the perovskite coverage; b) the shielding of the specific perovskite-TiO_2 interaction through functionalization, which is known to drive the preferential location of chloride-rich nucleation seeds. We demonstrated, through a cross analysis of the crystalline features and the photovoltaic performances of $CH_3NH_3PbI_{3-x}Cl_x$ films grown of functionalized and non-functionalized TiO_2 dense layer, that the crystalline order of the perovskite layer is not a priority condition for reaching high solar cells efficiency.
Insights gained from understanding the hybrid perovskite crystallization process and the film properties represent a step toward the rational design of the polycrystalline absorber film and TiO_2 interface modification.

Acknowledgements

VLPG, SC, AL, AR and GG acknowledge Progetto di ricerca PON R&C 2007-2013 (Avviso n. 713/Ric. del 29 ottobre 2010) MAAT-Molecular NAnotechnology for HeAlth and EnvironmenT (Project Number: PON02_00563_3316357), EFOR-Energia da FOntiRinnovabili (Iniziativa CNR per il Mezzogiorno L. 191/2009 art. 2 comma 44), Regione PUGLIA (APQ Reti di Laboratorio, project "PHOEBUS" cod. 31). SC and GG acknowledge the project Beyond-Nano (Project Number: PON03_00362) for financial support. The authors gratefully acknowledge Alessandra Zizzari and Dr. Valentina Arima for help with contact angle measurements, and Sonia Carallo for technical support.

Notes and references

[a] *Dipartimento di Matematica e Fisica "E. De Giorgi", Università del Salento, Via per Arnesano, 73100 Lecce, Italy*
[b] *Istituto di Cristallografia, CNR-IC, V. Amendola 122/O, 70126-Bari, Italy*
[c] *Center for Bio-Molecular Nanotechnology - Fondazione Istituto Italiano di Tecnologia, Via Barsanti, 73010 Arnesano (Lecce), Italy.*
[d] *CNR-IMM, Istituto per la Microelettronica e Microsistemi, Strada VIII n°5, 95121 Catania, Italy*
[e] *Università degli studi di Catania and INSTM UdR Catania, Viale Andrea Doria 6, 95125, Catania, Italy*
[f] *Istituto di Nanotecnologia, CNR-Nanotec, Polo di Nanotecnologia c/o Campus Ecotekne via Monteroni - 73100 Lecce, Italy*
* E-mail: aurora.rizzo@unisalento.it.

† Electronic Supplementary Information (ESI) available: Contact angle measurement of water on bare and NaPTH functionalized TiO_2 and perovskite absorption spectra. XPS onto bare TiO_2 and either DMOA and NaPTH functionalized TiO_2. GIWAXS 2D maps for the TiO_2 substrate and for full iodide perovskite $MAPbI_3$. Voltammograms onto bare TiO_2 and either DMOA and NaPTH functionalized TiO_2, See DOI: 10.1039/b000000x/

1. M. M. Lee, J. Teuscher, T. Miyasaka, T. N. Murakami, H. J Snaith, *Science* 2012, **338**, 643-647;
2. H. Zhou, Q. Chen, G. Li, S. Luo, T.-B. Song, Duan, Z. Hong, J. You, Y. Liu, Y. Yang, *Science* 2014, **345**, 542-546;
3. D. B. Mitzi, *Progress in Inorganic Chemistry* 2007, **48**, 1-121;
4. A. Dualeh, N. Tetreault, T. Moehlv, P. Gao, M. K. Nazeeruddin, M. Grätzel, *Adv. Funct. Mater.* 2014, **24**, 3250–3258;
5. K. W. Tan, D. T. Moore, M. Saliba, H. Sai, L. A. Estroff, T. Hanrath, H. J. Snaith, U. Wiesner, *ACS Nano* 2014, **8**, 4730–4739;
6. P. Docampo, F. C. Hanusch, N. Giesbrecht, P. Angloher, A. Ivanova, T. Bein *APL Mat.* 2014, **2**, 081508;
7. A. Ishii, A.-K. Jena, T. Miyasaka, *APL Mat.* **2014**, 2, 091102;
8. V. Trifiletti, V. Roiati, S. Colella, R. Giannuzzi, L. De Marco, A.Rizzo, M. Manca, A. Listorti, G. Gigli *ACS Appl. Mater. Interfaces*, **2015**, 7, 4283–4289;
9. S. Masi, S. Colella, A. Listorti, V. Roiati, A. Liscio, V. Palermo, A. Rizzo, G. Gigli, *Sci. Reports* **2015**, 5, 7725.
10. D. B. Mitzi, C. A. Feild, W. T. A. Harrison, A. M. Guloy, *Nature* **1994**, 369, 467 – 469.
11. D. B. Mitzi, K. Chondroudis, C. R. Kagan, *Inorg. Chem.* **1999**, 38, 6246-6256;
12. M. I. Dar, N. Arora, P. Gao, S. Ahmad, M. Grätzel, M. K. Nazeeruddin, *Nano Lett.* **2014**, 14, 6991-6996;
13. S. Colella, E. Mosconi, P. Fedeli, A. Listorti, F. Gazza, F. Orlandi, P. Ferro, T. Besagni, A. Rizzo, G. Calestani, G. Gigli, F. De Angelis, R. Mosca, *Chem. Mater.* **2013**, 25, 4613–4618;
14. M. Saliba, K.-W. Tan, H. Sai, D. T. Moore, T. Scott, W. Zhang, L. A. Estroff, U. Wiesner, H. J. Snaith, *J. Phys. Chem. C* **2014**, 118, 17171–17177;

15. Y. Tidhar, E. Edri, H. Weissman, D. Zohar, G. Hodes, D. Ca-hen, B. Rybtchinski, S. Kirmayer, *J. Am. Chem. Soc.* **2014**, 136, 13249–13256;
16. S. Colella, E. Mosconi, G. Pellegrino, A. Alberti, V. L. P. Guerra, S. Masi, A. Listorti, A. Rizzo, G. G., Condorelli, F. De Angelis, G. Gigli, *J. Phys. Chem. Lett.* **2014**, 5, 3532-3538;
17. V. Roiati, E. Mosconi, A. Listorti, S. Colella, G. Gigli, F. De Angelis, *Nano Lett.* **2014**, 14, 2168–2174;
18. G. E. Eperon, V. M. Burlakov, P. Docampo, A. Goriely, H. J. Snaith, *Adv. Funct. Mater.* **2014**, 24, 1, 151-157;
19. K. Wojciechowski, S. D. Stranks, A. Abate, G. Sadoughi, A. Sadhanala, N. Kopidakis, G. Rumbles, C.-Z. Li, R. H. Friend, A. K.-Y. Jen, H. J. Snaith, *ACS Nano*, **2014**, 8, 12701-12709;
20. Y. Ogomi, A. Morita, S. Tsukamoto, T. Saitho, Q. Shen, T. Toyoda, K. Yoshino, S. S. Pandey, T. Ma, S. Hayase, *J. Phys. Chem. C* **2014**, 118, 16651−16659;
21. N. Kitazawa, Y. Watanabe, Y. Nakamura, *J. Mater. Sci.* **2002**, 37, 3585–3587;
22. D. Altamura, R. Lassandro, F. A. Vittoria, L. De Caro, D. Siliqi, M. Ladisa, C. Giannini, *J. Appl. Cryst.*, **2012**, 45, 869;
23. B.-W. Park, B. Philippe, T. Gustafsson, K. Sveinbjörnsson, A. Hagfeldt, E. M. J. Johansson, G. Boschloo, *Chem. Mater.* **2014**, 26, 4466–4471;
24. S. T. Williams, F. Zuo, C.-C. Chueh, C.-Y. Liao, P.-W.; Liang, A. K.-Y. Jen, *ACS Nano* **2014**, 8, 10640–10654;
25. E. Mosconi, E. Ronca, F. De Angelis, *J. Phys. Chem. Lett.* **2014**, 5, 2619−2625.
26. T. Salim, S. Sun, Y. Abe, A. Krishna, A. C. Grimsdale, Y. M. Lam, *J. Mater. Chem.* **2015**, 3, 8943–8969.
27. Cho, C.-P.; Chu, C.-C.; Chen, W.-T.; Huang, T.-C.; Tao, Y.-T. *J. Mater. Chem.* **2012**, 22, 2915-2921.
28. A. Cacciuto, S. Auer, D. Frenkel, *Nature* **2004**, 428, 404-406;
29. S. K. Hau, H.-L. Yip, O. Acton, N. S. Baek, H. Ma, H.; A. K.-Y. Jen, *J. Mater. Chem.*, **2008**, 18, 5113–5119;
30. R. J. J. Jansen, H. Van Bekkum, *Carbon*, **1995**, 33, 1021-1027;
31. Y.-X. Ni, B. Feng, J. Wang, X. Lu, S. Qu, J. Weng, *J. Mater. Sci.* **2009**, 44, 4031–4039;
32. G. Pellegrino, G. G. Condorelli, F. De Rossi, T. M. Brown, F. Giovenale, C. Bongiorno, A. Alberti, *App. Surf. Sci.* **2014**, 296, 69–78;
33. H. P. Klug, L. E. Alexander, In X-Ray *Diffraction Procedures for Polycrystalline and Amorphous Materials Wiley & Sons*, **1973**, Section 9-3.1;
34. M. I. Dar, S. Sampath, S. A. Shivashankar, *Mater. Res. Express* **2014**, 1, 015025;
35. Q. Chen, H. Zhou, Y. Fang, A. Z. Stieg, T.-B. Song, H.-H. Wang, X. Xu, Y. Liu, S. Lu, J. You, P. Sun, J. McKay, M. S. Goorsky, Y. Yang, *Nature Comm.* **2015**, 6:7269**;**
36. Y.Bai, H. Yu, Z. Zhu, K. Jiang, T. Zhang, N. Zhao, S. Yang, H. Yan, *J. Mater. Chem. A* **2015**, 3, 9098–9102
37. M. Lee, Y. Jo, D. S. Kim, Y. Jun, *J. Mater. Chem. A* **2015**, 3, 4129-4133;
38. J. Troughton, D. Bryant, K. Wojciechowski, M. J. Carnie, Henry Snaith, D. A. Worsleya, T. M. Watson, *J. Mater. Chem. A*, **2015**, 3, 9141–9145;
39. G. Boschloo, D. Fitzmaurice*, J. Electrochem. Soc.* **2000**, 147, 1117–1123;
40. D. H. Taffa, M. Kathiresan, L. Walder, *Langmuir* **2009**, 259, 5371–5379
41. V. Roiati, S. Colella, G. Lerario, L De Marco, A. Rizzo, A. Listorti, G. Gigli, *Energy Environ. Sci.* **2014**, 7, 1889-1894.
42. T. Miyadera, Y. Shibata, T. Koganezawa, T. N. Murakami, T. Sugita, N. Tanigaki, M. Chikamatsu, *Nano Lett.* **2015**, 15, 5630−5634.
43. G. Pellegrino, S. Colella, I. Deretzis, G. G. Condorelli, E. Smecca, G. Gigli, A. La Magna, A. Alberti, *J. Phys. Chem. C* **2015**, 119 19808–19816.